American Mineralogist, Volume 85, pages 698–706, 2000

Crystal chemistry of the axinite-group minerals: A multi-analytical approach

GIOVANNI B. ANDREOZZI,[1,*,†] LUISA OTTOLINI,[2] SERGIO LUCCHESI,[1] GIORGIO GRAZIANI,[1] AND UMBERTO RUSSO [3]

[1]Dipartimento di Scienze della Terra, Università di Roma "La Sapienza," Piazzale Aldo Moro 5, I-00185 Roma, Italy
[2]C.N.R. Centro di Studio per la Cristallochimica e la Cristallografia, Via Ferrata 1, I-27100 Pavia, Italy
[3]Dipartimento di Chimica Inorganica, Metallorganica e Analitica, Università di Padova, Via Loredan 4, I-35131 Padova, Italy

ABSTRACT

Sixty axinite samples from 24 localities worldwide were characterized by electron microprobe analysis (EMPA) to define the limits of compositional variation. Three samples are very close to the Mn, Fe, and Mg end-members. Ternary (Mn,Fe^{2+},Mg)-compositions occur mostly in the ferroaxinite and manganaxinite fields, and are constrained by the relation Mg ≤ Fe. Core-rim chemical zoning was observed in 20 samples, with systematic enrichment of Fe in the core and Mn in the rim, independent of sample provenance.

The chemical composition (including B, H, and Fe^{2+}/Fe^{3+}) of 17 homogeneous samples was investigated using electron-microprobe analysis, thermo-gravimetry (TG), ion microprobe (SIMS), crystal-structure refinement (SREF), and Mössbauer spectroscopy (MS). For all samples except pure manganaxinite, most of the iron is Fe^{2+}. The content of Fe^{3+} and the $Fe^{3+}/\Sigma Fe$ ratio increase with Mn content up to 0.31 atoms per formula unit (apfu) and 0.80, respectively. Fe^{3+} may substitute for Al or also for divalent cations balanced by the OH deficiency:

$$Fe^{3+} + O^{2-} \leftrightarrow Fe^{2+} + OH^{-}, \text{ or } Fe^{3+}O(Fe^{2+}OH)_{-1}$$

Boron content ranges from 1.88 to 2.07 apfu (±2.5% relative) and shows an inverse relation with Si content. Direct measurement of the *B*-tetrahedron size provides structural confirmation of the Si ↔ B exchange. Hydroxyl deficiency accompanies this substitution and the following coupled mechanism is proposed:

$$Si^{4+} + O^{2-} \leftrightarrow B^{3+} + OH^{-}, \text{ or } SiO(BOH)_{-1}$$

Hydrogen content ranges from 1.7 to 2.1 apfu (±5% relative). The deficiency of OH from the stoichiometric value of 2.0 per formula unit is related directly to the number of trivalent and tetravalent cations, as OH content plays a crucial role in charge-balance relations.

A revised *chemical* formula for the axinite-group minerals is proposed:

$$^{[6]}[Ca(Ca_{1-x}Mn_x)(Mn,Fe^{2+},Mg,Zn,Al_u,Fe^{3+}_v)_{\Sigma=1}(Al_{2-y}Fe^{3+}_y)]_2{}^{[4]}[(B_{1-z}Si_z)_2Si_8]O_{30}(OH_{1-w}O_w)_2,$$

where $x \leq 1$, $u < 1$, $v < 1$, $y < 1$, $z << 1$, and $w = (u + v + z)$.

INTRODUCTION

The axinite-group minerals $(Ca,Mn)_4(Mn,Fe,Mg)_2(Al,Fe)_4B_2Si_8O_{30}(OH)_2$ are complex phases typically occurring in low- to medium-grade metamorphic environments (Grew 1996). As they are in some cases the only borosilicates in regionally metamorphosed rocks, axinites are believed to be the alternative phase to tourmaline in Al-poor, Ca-rich parageneses (Pringle and Kawachi 1980). However, notwithstanding their occurrence over a wide range of environments and in spite of their high compositional flexibility and sensitivity to P-T-X-f_{O_2} conditions, axinites have not been extensively studied.

Their crystal structure, with $P\bar{1}$ symmetry, may be described as a sequence of tetrahedrally and octahedrally coordinated cations (Ito et al. 1969; Takéuchi et al. 1974). Two disilicate groups $[Si_2O_7]$ are connected by two BO_4 tetrahedra to form a six-membered ring. Two additional disilicate groups share corners with the BO_4 tetrahedra, forming a $[B_2Si_8O_{30}]$ planar cluster. Slightly distorted octahedra, four filled by Al and two by

*E-mail: graziani@uniroma1.it
†Present address: Dip. Mineralogia e Petrologia, Corso Garibaldi 37, 35137 Padova, Italy.

0003-004X/00/0506–698$05.00

Mn-Fe-Mg, share edges to form a six-membered finite chain. Connection among these chains is provided by strongly distorted octahedra CaO_6 and $(Ca,Mn)O_5(OH)$. This infinite octahedral framework contains the $[B_2Si_8O_{30}]$ groups.

Sanero and Gottardi (1968) proposed the general formula and the nomenclature now commonly accepted for axinite. For compositions in which Ca is close to 4 atoms per formula unit (apfu), the end-members are *manganaxinite*, *ferroaxinite*, and *magnesioaxinite*. *Tinzenite* has a Ca deficiency ($2 < Ca < 4$) that is compensated by an excess of Mn, which is ordered in the smaller of the two sites occupied by Ca (Basso et al. 1973). Lumpkin and Ribbe (1979) proposed a structural formula for axinite-group minerals based on 32 (O,OH) anions: $^{[6]}[(Mn,Fe^{2+},Mg,Zn,Al_w)(Ca_{2-x}Mn_x)(Al_{2-y}Fe^{3+}_y)]_2(OH_{2-w}O_w)$ $^{[4]}(B_2Si_{8-z}Al_z)O_{30}$, where $w < 1$, $x < 1$, $y << 1$, and $z << 1$. This formula needs further improvement because: (a) the amount *w* of O does not balance the amount 2*w* of Al; (b) no structural evidence was presented to support the substitution of Al for Si at the tetrahedral sites, and (c) occupancy and dimensional differences between independent octahedra were not considered. In fact, the formula ignores the ordering of excess Mn, as in the case of tinzenite-rich manganaxinites (Basso et al. 1973), as well as the possibility of different populations in the two independent Al-octahedra.

The characterization of axinite compositions is complicated because of the need to determine the Fe^{3+}/Fe^{2+} ratio and to quantify B and H. Mössbauer spectroscopy has shown most of the Fe in axinite to be Fe^{2+} (Takashima and Ohashi 1968; Astakhov et al. 1975; Pieczka and Kraczka 1994). Light elements (B, H, etc.) play an important role in borosilicate minerals, so that the lack of information due to the common assumption of their stoichiometric content may affect the validity of proposed crystal-chemical relations (Hawthorne 1996). Until a few years ago, quantitative measurement of B and H in minerals was not straightforward, with the result that most published chemical analyses of axinite are incomplete (Chaudhry and Howie 1969; Lumpkin and Ribbe 1979; Deer et al. 1986). Recent improvements in the quantification of light elements in silicate matrices by secondary ion mass spectrometry (SIMS) (Ottolini et al. 1993, 1995) together with electron-microprobe analysis (EMPA), thermo-gravimetry (TG), X-ray diffraction (XRD), structure refinement (SREF), and Mössbauer spectroscopy (MS), provide a multi-analytical approach for complete chemical characterization of common silicates, allowing quantification of light elements with good accuracy (Černý et al. 1995; Hawthorne et al. 1995; Andreozzi 1997; Federico et al. 1998).

Experimental procedures

This work is based on 60 samples collected from 24 localities worldwide (Table 1). In most cases the paragenesis was not known and in few cases also the provenance was largely undetermined. The samples were idiomorphic axe-shaped crystals of millimeter size, with a vitreous aspect and low to medium transparency, variously colored purple-red, brown, yellow-green, and pale blue. Their chemical compositions and zoning were characterized by EMP traverses from core to rim. Seventeen homogeneous crystals were selected for detailed study.

Table 1. Localities and sources of axinites used in this study

Sample no.	Locality	Source
1	Bourg d'Oisans, Isère, France	MMR 7239/1
2	Bourg d'Oisans, Isère, France	MMR 7240/2
3	Bourg d'Oisans, Isère, France	MMR 7241/3
4	Bourg d'Oisans, Isère, France	MMR 7242/4
5	Bourg d'Oisans, Isère, France	MMR 7243/5
6	Bourg d'Oisans, Isère, France	MMR 7244/6
7	Bourg d'Oisans, Isère, France	MMR 7245/7
8	Bourg d'Oisans, Isère, France	MMR 7246/8
9	Bourg d'Oisans, Isère, France	MMR 7247/9
10	Bourg d'Oisans, Isère, France	MMR 7248/10
11	Bourg d'Oisans, Isère, France	MMR 7249/11
12	Bourg d'Oisans, Isère, France	MMR 7250/12
13	Skopi, St. Gotthard, Switzerland	MMR 7251/13
14	Skopi, St. Gotthard, Switzerland	MMR 7252/14
15	Skopi, St. Gotthard, Switzerland	MMR 7253/15
16	Chamonix, France	MMR 7254/16
17	Chamonix, France	MMR 7255/17
18	Skopi, St. Gotthard, Switzerland	MMR 7256/18
19	Treseburg, Harz Mt., Germany	MMR 7257/19
20	Botallack, Cornwall, England	MMR 7258/20
21	Botallack, Cornwall, England	MMR 7259/21
22	Miask, Polar Ural Mt., Russia	MMR 7260/22
23	Bourg d'Oisans, Isère, France	MMR 7261/23
24	Striegau, Silesia, Poland	MMR 13984/24
25	Striegau, Silesia, Poland	MMR 13985/25
26	Striegau, Silesia, Poland	MMR 17762/26
27	Striegau, Silesia, Poland	MMR 17763/27
28	Striegau, Silesia, Poland	MMR 17764/28
29	Skopi, St. Gotthard, Switzerland	MMR 17855/29
30	Rosebery, Tasmania, Australia	MMR 21020/30
31	Obira, Bungo, Japan	MMR 2166/31
32	Obira, Bungo, Japan	MMR 21332/32
33	Obira, Bungo, Japan	MMR 22055/33
34	Obira, Bungo, Japan	MMR 22056/34
35	S. Paolo Cervo, Biella, Italy	MMR 22293/35
36	Jama-Ura, Bungo, Japan	MMR 22460/36
37	Obira, Bungo, Japan	MMR 22553/37
38	Hajikami, Japan	MMR 22670/38
39	Botallack, Cornwall, England	MMR 23067/39
40	Zbraslav, Prague, Czech Rep.	MMR 24199/1
41	Gambatesa, Chiavari, Italy	MMR 23711/1
42	Gambatesa, Chiavari, Italy	MMR 23862/2
43	Lavagna, Chiavari, Italy	MMR 23945/3
44	Lavagna, Chiavari, Italy	MMR 23946/4
45	Lavagna, Chiavari, Italy	MMR 23947/5
46	Luning, Nevada, US	NHMSI 94407/4
47	Graham, Arizona, US	R. Allori
48	Dalnegorsk, Vladivostok, Russia	R. Allori
49	Bourg d'Oisans, Isère, France	R. Allori
50	Bourg d'Oisans, Isère, France	R. Allori
51	Lower Pareora Gorge, N. Zealand	OU 44672
52	Dansey Pass, N. Zealand	OU 25336
53	Upper Wakatipu, N. Zealand	OU 33366
54	Sri Lanka	M. C. de S. Jayasekera
55	Tanzania	J. Saul
56	Tanzania	J. Saul
57	Tanzania	J. Saul
58	Dalnegorsk, Vladivostock, Russia	L. Caserini
59	Puywa, Subpolar Ural Mt., Russia	L. Caserini
60	Chukotka, Russia	M. Burli

Notes: MMR = Museum of Mineralogy, University of Rome "La Sapienza", Italy.
NHMSI = Natural History Museum, Smithsonian Institution, Washington, D.C., U.S.
OU = Otago University, Dunedin, New Zealand.

X-ray diffraction and structure refinement

The seventeen chemically homogeneous crystal fragments were cut into ~0.3 mm edge cubes. X-ray data collection was done on a Siemens P4 single-crystal four-circle automated diffractometer with Mo$K\alpha$ radiation in the range 3–65° 2θ. After corrections for Lorentz effects, polarization, and absorption, crystal structures were refined in $P\bar{1}$ to R indices ranging from 1.88 to 2.65%. The SHELXTL-PC program package was used and the refined variables were scale factor, isotropic-extinction coefficient, site occupancies, and positional and anisotropic displacement parameters. Initial structural parameters were taken from Takéuchi et al. (1974). Full details will be given elsewhere (Andreozzi et al. unpublished manuscript).

Thermo-gravimetry

Some bulk homogeneous samples (samples 22, 26, 38, 47, 54, and 58; see Table 1) were powdered and prepared for thermal analysis with a Setaram TAG 24 operating with the following conditions: range 20–1100 °C, heating rate 10 °C/min, N_2 atmosphere, sample weight about 10 mg, alumina crucible, calcined alumina as inert material. The volatile phase, released from 600 to 1000 °C, was characterized by means of gas chromatography, which revealed only H_2O and traces of CO_2. The accuracy and reproducibility of TG measurements was about 5% (relative), with K_2CO_3 as a test-material.

Electron-microprobe analysis

The crystals used for SREF were analyzed for elements with Z ≥ 9 by a Cameca SX-50 operating with five wavelength-dispersive spectrometers (WDS) and a Link eXL energy-dispersion system (EDS), both controlled by Specta software, at the "Centro di Studio per il Quaternario e l'Evoluzione Ambientale" C.N.R., Rome. Data were reduced with ZAF-4/FLS software. Operating conditions were as follows: accelerating voltage 15 kV, sample current 15 nA, 100 and 20 s counting time for EDS and WDS determinations, respectively. Natural and synthetic standards used were: wollastonite (Si, Ca), corundum (Al), jadeite (Na), periclase (Mg), fluorphlogopite (F), magnetite (Fe), orthoclase (K), rutile (Ti), and metals (Mn, Cr, and Zn). A signal was considered detected only if its intensity was twice as large as its standard deviation. Analytical errors were in the range of 1% (relative) for major elements and 5% (relative) for minor elements.

Ion microprobe analysis

Analysis for H and B was done on the same crystal fragments with a Cameca IMS 4f ion microprobe at C.N.R.-CSCC, Pavia. The $^{16}O^-$ primary ion beam was used and secondary ions H^+, $^{11}B^+$, and $^{30}Si^+$ were collected under the experimental conditions described in Ottolini and Hawthorne (1999). Lithium was investigated as $^7Li^+$ secondary ions and its content turned out to be negligible (≤5 ppm in the whole sample set).

Boron quantification. Analysis of light elements by SIMS using low-energy ions, for which the secondary ion intensities are more intense, is generally affected by quite large matrix effects, and the relation between ion intensity and corresponding elemental concentration is very often non-linear. Matrix effects were reduced and reproducibility improved using high-energy ions (Ottolini et al. 1993): the variation of the ion yield for B with respect to Si, IY(B/Si), with ^{30}Si selected as the matrix-reference element, proved to be of the order of ~10% (relative) over a wide compositional range. Moreover, accurate B analyses ≤ 3% (relative) could be obtained by a regression line: IY(B/Si) vs. (Fe+Mn) (in cation%) for each sample (Ottolini and Hawthorne 1999).

In the present work, for high accuracy of B analysis in axinites, a specific calibration curve was constructed. The reference samples were: two Fe-rich tourmalines (L1v and L3l, Table 2) previously characterized by SREF, EMPA, and SIMS (Federico et al. 1998; Lucchesi et al., unpublished manuscript); Pyrex glass (B_2O_3 12.86 wt%, SiO_2 80.61 wt%), taken as representative of the working curve used by Ottolini et al. (1993); one Mn-rich tourmaline (2G, Table 2) and three axinites (A, B, and E, Table 2). The boron concentration of 2G tourmaline was measured by SIMS (Lucchesi et al., unpublished manuscript), and that of the three axinite samples was derived by stoichiometry (EMP analysis by F.C. Hawthorne, unpublished data). The regression coefficient of the present working curve was R^2 = 0.99. The deviation of all experimental points from the curve was small (≤5%), suggesting that residual matrix effects in this compositional range are rather small. The precision of SIMS measurements, derived from the reproducibility of analysis on Pyrex, was of the order of ~2.5% (2σ) over a one-day span.

Hydrogen quantification. An accuracy of 15% (relative) was first obtained for SIMS measurements of H in various silicates with low- to medium-silica content and H_2O > 0.1 wt%, using a calibration curve made of cordierite, amphibole, and basalt standards (Ottolini et al. 1995). To better evaluate matrix effects in axinites, a specific working curve was constructed. Due to lack of suitable standards with matrix comparable to axinites, the H_2O contents of samples 26, 38, 54, and 58 were measured by TG. These four axinites (Table 3) and one tourmaline, the L3l schorl (Federico et al. 1998) represented the standards for the working curve. Axinite E, with H_2O content derived by stoichiometry, was introduced for comparison. The agreement with the derived working curve was within 5% (relative). Reproducibility of H analysis on the axinites was better than 3–4% (1σ %) during an analytical session of one day.

To test the applicability of the present working curve to Fe- and Mn-rich axinites, two more samples—axinite 47 (belonging to the present set of axinites, see Table 3) and tourmaline L1v (Table 2)—were analyzed. Their reference H_2O contents were derived by TG. Axinite 47 and L1v showed an IY(H/Si)

TABLE 2. Composition of standard and reference samples

No.	1	2	3	4	5	6
SiO_2	34.70	35.28	36.11	42.03	41.60	42.31
FeO	14.45	11.59	0.00	7.86	8.07	6.53
MnO	0.26	0.15	9.65	4.00	1.98	2.63
B_2O_3	9.60	10.22	10.24	6.06	6.07	6.14
H_2O	3.02	2.99	–	–	–	1.59

Notes: Only oxide concentrations used for SIMS calibration are reported. 1 = Llv(Fe-rich tourmaline); 2 = L3l(Fe-rich tourmaline); 3 = 2G (Mn-rich tourmaline); 4 = Ax A (Axinite); 5 = Ax B (axinite); 6 = Ax E (axinite).

lower by ~20 and 10% (relative), respectively, than that defined by the working curve derived here for axinites [IY(H/Si) = 1.73]. We believe that such a discrepancy is mostly due to residual matrix effects related to the higher (Fe+Mn) content of these samples (see Tables 2 and 3). The present set of data supports the existence of an inverse correlation between IY(H/Si) and the (Fe + Mn) content in the sample, similar to that in the SIMS analysis of H in schorl (Aurisicchio et al. 1999) and that found for Li and B in schorl-elbaitic tourmalines (Ottolini and Hawthorne 1999). In particular, axinite 47, which shows the highest matrix effects, also has the highest Mn content (MnO = 12.5 wt%) and its Fe is present mostly as Fe^{3+} (Table 3).

Mössbauer spectroscopy

Samples were prepared by finely grinding about 20 mg of material in an agate mortar under acetone; the powder was then suspended in Vaseline, placed in a lead container, and wrapped in thin plastic foil. Spectra were acquired both at room temperature and low temperature (liquid N) using a constant-acceleration spectrometer with a symmetrical waveform and a ^{57}Co source (nominal strength 1.4 MBq) in a Rh matrix. The spectrometer was calibrated with natural abundance α-Fe foil at room temperature. Mirror-symmetric spectra were accumulated in a 512-channel analyzer, folded, and fitted to pure Lorentzian line-shapes with the aid of a least-squares fitting program. The percentages of Fe^{2+} and Fe^{3+}, with respect to total-Fe content, were established by measuring the integrated area of the absorption peaks (with an estimated absolute error of ±2%). Details of MS spectra and discussion about Fe^{2+}- and Fe^{3+}-ordering in axinite will be given elsewhere (Andreozzi et al. in preparation).

RESULTS

Axinite chemistry and compositional zoning

The ternary Mn-Fe^{2+}-Mg diagram (Fig. 1) shows the compositional variation of the 60 axinites. Ferroaxinites almost completely occupy their sub-field, with the exception of the area close to the end-member, and show continuous solid solution toward manganaxinite. Manganese-rich samples occupy only half of their sub-field (the Mg-poor area) and seem to be less common than ferroaxinite. Mg-rich samples are represented only by the end-member and a few points close to the boundary between magnesio- and ferroaxinite. In general, there is an absence of compositions throughout the field of magnesioaxinite. The substitutions may be expressed by the vector method (Burt 1989). With ferroaxinite, $Ca_4Fe^{2+}_2Al_4B_2Si_8O_{30}(OH)_2$, as the additive component, the main cation substitutions correspond to $MnFe^{2+}_{-1}$ and $MgFe^{2+}_{-1}$.

The compositions of the samples studied closely overlap the chemical data of all known axinites reviewed by Grew (1996). In particular, the transparent yellow-green manganaxinite (no. 47), the purple-red ferroaxinite (no. 54), and the pale-blue magnesioaxinite (no. 56) have chemical compositions very close to the axinite-group end-members (Fig. 2). Therefore, the samples studied may be considered representative of the compositional space known so far (cf. Lumpkin and Ribbe 1979; Deer et al. 1986; Grew 1996).

The distribution of data in Figure 1 suggests the presence of a compositional gap between Mn and Mg end-members, as already supposed by Chaudhry and Howie (1969) and Pringle and Kawachi (1980). The absence of solid solution between manganaxinite and magnesioaxinite may be due to (1) the scarcity of rocks simultaneously enriched in Mn, Mg, and B, and impoverished in Fe, and (2) the tendency of axinites to fractionate Mn and Fe (Grew 1996). However, in Mn-rich samples, an increase in Mg content is usually accompanied by an increase in Fe^{2+} content, so that the upper limit for the manganaxinite analyses corresponds closely to the Mg = Fe^{2+} line. The amount of Mg accepted in the axinite structure when Mn is present thus seems to be constrained by the Fe^{2+} content. The geometrical deformation of the large octahedron in which Mn, Fe^{2+}, and Mg occur plays an important role in the structural control of the hypothesized miscibility gap (Andreozzi et al., unpublished manuscript).

Twenty samples—with different provenance—showed distinct core-rim chemical zoning, characterized by Mn enrichment at the rim. All samples display the same zoning trend from ferro- to manganaxinite from core to rim (Figs. 3 and 4). The zoning is of two types: the first and more common variety is characterized by a large Fe-rich core and a narrow Mn-rich rim (Fig. 3a); the second variety, which is relatively rare, involves a very small Fe-rich core surrounded by a large Mn-rich rim (Fig. 3b). The first type was generally observed in ferroaxinites and the second in some manganaxinites. Moreover, (Fe,Mg)-rich samples show Mg depletion at the rim.

Complete chemical data for the 17 homogeneous samples are shown in Table 3, and compositions are plotted in Figure 2. For all samples, total cations are close to 20 apfu. Calcium contents range from 3.84 to 3.96 apfu (tinzenite-rich samples with 2 < Ca < 4 apfu were excluded from this study). The mi-

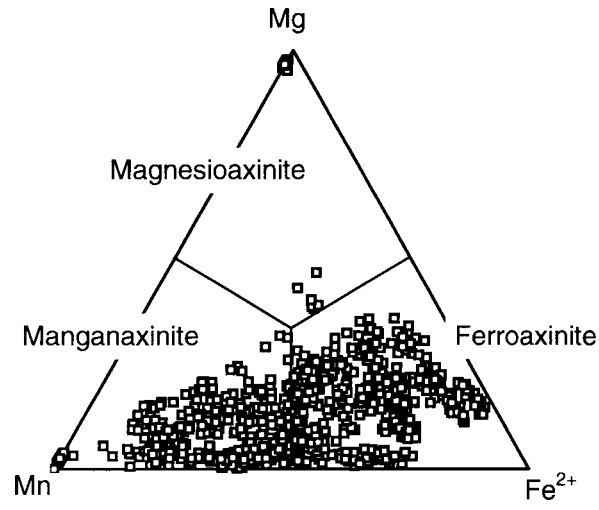

FIGURE 1. Ternary diagram showing Mn-Fe^{2+}-Mg contents of axinites [normalized to (Mn + Fe^{2+} + Mg) = 1]. More than 1000 compositions of 60 specimens from 24 localities worldwide are plotted. They closely overlap all analyzed axinites reported by Grew (1996).

TABLE 3. Chemical composition of representative axinite samples. Average oxide weight percentages and standard deviations (1σ) of four EMP analyses

Ax no.	1	3	14	22	26[a]	28[b]	30	33[c]	35[d]
SiO_2	42.3(2)	42.7(4)	42.5(2)	42.6(3)	42.4(2)	42.3(2)	41.7(4)	42.9(3)	42.8(2)
B_2O_3*	6.1(2)	6.3(2)	5.9(2)	6.3(2)	5.7(1)	5.8(2)	6.3(2)	6.0(2)	6.0(2)
Al_2O_3	17.9(2)	17.9(1)	17.96(7)	18.06(9)	17.6(2)	17.8(2)	17.5(2)	17.8(2)	17.3(2)
FeO	4.9(2)	7.12(6)	8.5(1)	8.1(4)	6.1(3)	6.7(2)	9.4(1)	2.12(7)	6.5(3)
MgO	1.21(3)	2.06(7)	1.56(8)	2.03(5)	0.15(2)	0.38(2)	0.74(3)	1.07(6)	1.4(1)
MnO	6.15(7)	2.3(1)	1.8(1)	1.3(8)	6.8(4)	5.5(2)	2.88(5)	9.8(2)	5.1(4)
CaO	19.3(1)	19.36(8)	19.44(8)	19.4(2)	19.1(2)	19.18(8)	19.06(9)	19.27(9)	19.28(8)
H_2O†	1.5(1)	1.3(1)	1.4(1)	1.6(1)	1.5(1)	1.4(1)	1.3(1)	1.6(1)	1.6(1)
Tot	99.4	99.0	99.1	99.4	99.4	99.1	98.9	100.6	100.0
FeO‡	4.4(1)	5.5(4)	7.2(3)	8.1(6)	5.7(1)	6.1(1)	8.3(2)	1.79(4)	5.5(1)
Fe_2O_3‡	0.6(1)	1.8(4)	1.5(3)	0.0(6)	0.3(1)	0.7(1)	1.3(2)	0.36(4)	1.1(1)
Number of ions on the basis of 32 (O,OH)									
Si	8.00(1)	8.03(2)	8.04(3)	8.00(2)	8.10(2)	8.08(3)	7.98(2)	8.06(1)	8.04(2)
B	2.00(5)	2.04(5)	1.94(5)	2.04(5)	1.88(5)	1.91(5)	2.07(5)	1.95(5)	1.93(5)
Al	4.00(2)	3.97(1)	4.01(2)	4.00(2)	3.98(4)	3.99(3)	3.94(2)	3.93(3)	3.84(4)
Fe^{3+}	0.08(2)	0.25(5)	0.21(4)	0.00(8)	0.05(2)	0.10(2)	0.19(3)	0.05(1)	0.16(2)
Fe^{2+}	0.69(2)	0.86(5)	1.13(4)	1.27(8)	0.91(2)	0.97(2)	1.32(3)	0.28(1)	0.86(2)
Mg	0.34(1)	0.58(2)	0.44(2)	0.57(1)	0.04(1)	0.11(1)	0.21(1)	0.30(2)	0.40(4)
Mn	0.98(5)	0.37(3)	0.29(2)	0.21(4)	1.10(4)	0.89(4)	0.47(3)	1.55(4)	0.81(4)
Ca	3.91(3)	3.90(1)	3.94(1)	3.90(3)	3.92(3)	3.93(1)	3.91(2)	3.87(2)	3.88(2)
OH	1.9(1)	1.7(1)	1.8(1)	2.0(1)	1.9(1)	1.8(1)	1.7(1)	1.9(1)	2.0(1)
Tot§	20.00	20.00	20.00	20.00	20.00[a]	20.00[b]	20.09	20.01[c]	19.95[d]

Notes: [a]Includes Zn 0.02. [b]Includes Zn 0.02. [c]Includes Zn 0.02. [d]Includes Ti 0.03. All values in apfu.
*From SIMS.
†From SIMS, except samples 22 and 26, measured by TG and used for SIMS calibration.
‡From Mössbauer data, except samples 1, 3, 14, 22, 28 (calculated by charge balance).
§Excluding OH.
F and K not detected.

nor Ca deficiency is balanced by excess Mn (Basso et al. 1973). As tinzenite, $Ca_2Mn_4Al_4B_2Si_8O_{30}(OH)_2$, forms a solid solution with manganaxinite $Ca_4Mn_2Al_4B_2Si_8O_{30}(OH)_2$, the latter was taken as the additive component to which exchange vector $MnCa_{-1}$ may be applied. The content of Zn was always low (≤0.03 apfu) but was more commonly found in manganaxinites than in ferroaxinites, as already observed by Lumpkin and Ribbe (1979). The amount of Al ranged from 3.73 to 4.05 apfu; its deficiency, according to Astakhov et al. (1975) and Lumpkin and Ribbe (1979), is balanced by Fe^{3+} (samples 47 and 48).

Boron and hydrogen contents

The B contents range from 1.88 to 2.07 apfu and Si contents range from 7.98 to 8.10 apfu (Table 3). Although no crystal-chemical relation had been known previously between B and Si in axinite, comparison of B and Si showed a significant inverse linear relation, suggesting Si → B substitution (Fig. 5). If the scatter of B measurements around the stoichiometric value of 2 apfu were only due to error, no such correlation would be expected; this was the case for every element except Si. Moreover, it should be pointed out that the procedure to obtain B_2O_3 from the B^+/Si^+ ion-intensity ratio includes calibration on SiO_2 content for each sample. As a consequence, any inaccuracy in SiO_2 measured by EMPA will affect the final B quantification. However, the observed correlation is inverse, so that such a dependency may be excluded. Therefore, for Si contents > 8.00 apfu, Si substitution for B (up to 0.10 apfu) is inferred. The inverse substitution of B for Si at the *Si*(1–4) sites, suggested

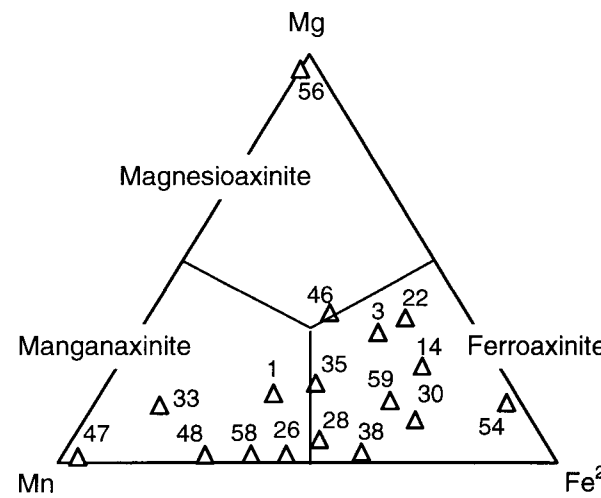

FIGURE 2. Ternary diagram showing Mn-Fe^{2+}-Mg contents [normalized to (Mn + Fe^{2+} + Mg) = 1] of 17 selected axinites characterized by EMPA, SIMS, TG, SREF, and MS. Symbol size corresponds to about ±1σ of cation contents.

TABLE 3 — *Extended*

Ax no.	38	46[e]	47	48[f]	54[g]	56[h]	58[i]	59
SiO_2	42.3(1)	43.1(2)	41.8(2)	42.3(2)	42.1(4)	44.8(2)	42.8(5)	43.3(6)
B_2O_3*	6.1(2)	6.0(2)	6.0(2)	6.1	6.3(2)	6.5(2)	6.1(2)	5.9(2)
Al_2O_3	17.8(2)	18.0(1)	16.7(3)	16.7(1)	17.7(2)	18.9(3)	18.2(2)	18.4(3)
FeO	8.7(4)	4.83(7)	2.3(4)	5.0(6)	10.60(7)	0.00	5.5(9)	8.1(2)
MgO	0.19(4)	2.75(2)	0.00	0.13(5)	1.07(4)	7.18(1)	0.14(3)	1.07(4)
MnO	4.7(2)	3.7(1)	12.5(2)	9.2(5)	0.4(1)	0.5(1)	7.8(9)	3.30(4)
CaO	18.9(2)	19.7(1)	18.7(1)	19.2(1)	19.38(7)	20.6(1)	19.4(3)	19.5(1)
H_2O†	1.4(1)	1.6(1)	1.4(1)	1.7(1)	1.6(1)	1.6(1)	1.6(1)	1.4(1)
Tot	100.1	99.7	99.4	100.4	99.2	100.1	101.5	101.0
FeO‡	7.3(2)	4.8(1)	0.41(5)	3.8(1)	10.6(2)	0.00	4.8(1)	7.4(1)
Fe_2O_3‡	1.5(2)	0.0(1)	2.15(5)	1.4(1)	0.0(2)	0.00	0.8(1)	0.7(1)
				Number of ions on the basis of 32 (O,OH)				
Si	8.01(1)	8.04(2)	8.02(3)	8.01(2)	7.99(2)	8.04(4)	8.01(2)	8.08(4)
B	1.99(5)	1.95(5)	1.99(5)	2.0	2.07(5)	2.00(5)	1.95(5)	1.91(5)
Al	3.98(4)	3.96(1)	3.76(6)	3.73(2)	3.95(1)	4.00(3)	4.01(2)	4.05(4)
Fe^{3+}	0.22(3)	0.00	0.31(1)	0.19(2)	0.00	0.00	0.11(2)	0.10(2)
Fe^{2+}	1.16(3)	0.75(2)	0.07(1)	0.60(2)	1.68(3)	0.00	0.76(2)	1.16(2)
Mg	0.05(1)	0.77(1)	0.00	0.04(1)	0.30(1)	1.92(1)	0.04(1)	0.30(1)
Mn	0.75(1)	0.58(1)	2.02(2)	1.5(1)	0.06(2)	0.07(2)	1.2(2)	0.52(2)
Ca	3.84(3)	3.94(1)	3.87(3)	3.90(2)	3.94(3)	3.96(3)	3.89(2)	3.88(2)
OH	1.8(1)	2.0(1)	1.8(1)	2.1(1)	2.0(1)	1.9(1)	1.9(1)	1.8(1)
Tot§	20.00	20.00[e]	20.04	20.00[f]	20.01[g]	20.03[h]	19.98[i]	20.00

Notes: [e]Includes Zn 0.01. [f]Includes Zn 0.03. [g]Includes Zn 0.01 and Na 0.01. [h]Includes V^{3+} 0.03 and Cr^{3+} 0.01. [i]Includes Zn 0.01. All values in apfu.
*From SIMS, except sample 48 (SIMS data not available, B calculated by charge balance).
†From SIMS, except samples 38, 47, 54, and 58, measured by TG and used for SIMS calibration.
‡From Mössbauer data, except sample 59 (calculated by charge balance).
§Excluding OH.
F and K not detected.

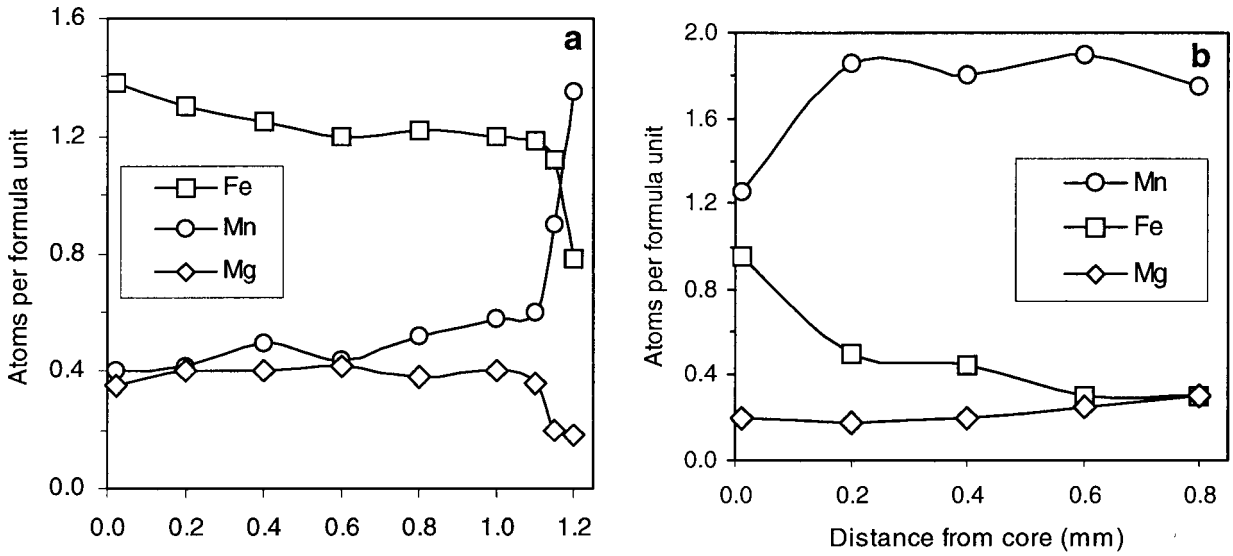

FIGURE 3. Chemical zoning observed from core to rim in some axinite specimens: (**a**) typical trend observed in most zoned samples: ferroaxinite (sample 15); (**b**) typical trend observed in some zoned samples: manganaxinite (sample 37).

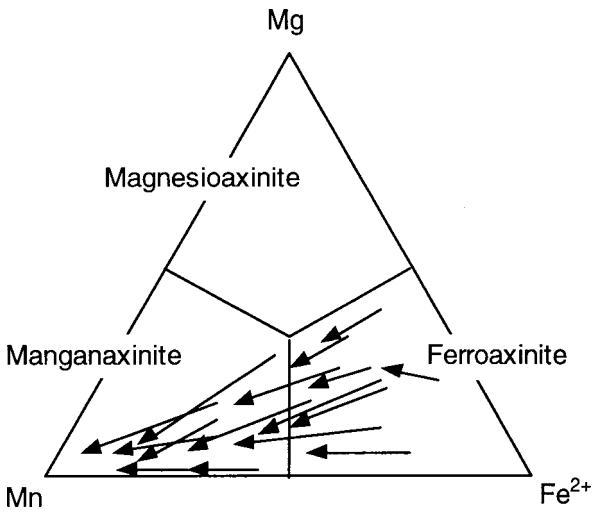

FIGURE 4. Core-rim zoning in axinite shown by arrows connecting mean-core composition with mean-rim composition of zoned samples. For each sample, the length of the arrow is proportional to the extent of chemical zoning. For simplification, only the most zoned cases are shown.

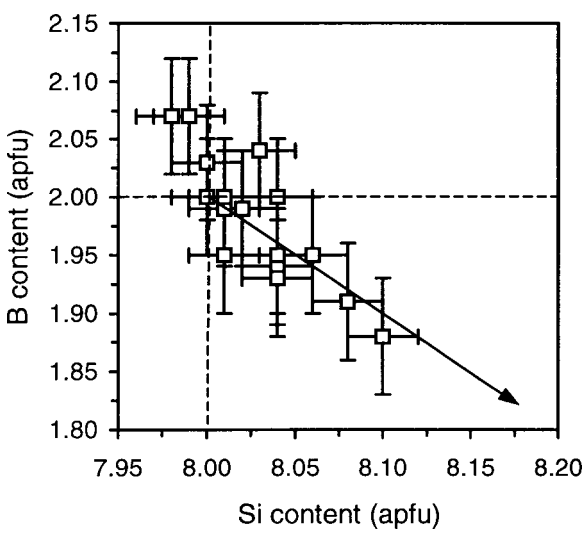

FIGURE 5. B vs. Si contents of studied axinites. Error bars: ±1σ for both B and Si. Horizontal and vertical dashed lines: stoichiometric values of 2 apfu (for B) and 8 apfu (for Si), respectively. Solid line with slope of –1 shows the ideal Si → B substitution.

by the few points with high-B and low-Si values (samples 30 and 54, Fig. 5), is more difficult to corroborate, as these data fall close to the stoichiometric values for B and Si.

The OH contents range from 1.7 to 2.1 apfu (Table 3). Samples 3, 14, 28, 30, 38, 47, and 59 are characterized by OH ≈ 1.8 apfu and have excess Si and/or trivalent cations. All other samples have OH ≈ 2 apfu. Unusually low H_2O contents of 1.1 and 1.2 wt% were obtained for samples 47 and 22, although a TG check on the same samples gave 1.4(1) and 1.6(1) wt% (Table 3). The TG values are more reasonable, as they give OH contents closer to bulk-chemistry requirements and are in line with the observed compositions of all other samples. Due to the high (Fe+Mn) contents of samples 47 and 22, the low-H values are probably related to matrix effects. Matrix effects for H/Si in tourmalines of schorl-elbaitic compositions were investigated by Ottolini and Hawthorne (1999). The variation of the IY(H/Si) with respect to (Fe+Mn) content resulted to be comparable with the uncertainty of the derived H/Si working curve (±10% relative). Matrix effects, if they exist, are therefore of this order. Moreover, the decrease of IY(H/Si) as a function of (Fe+Mn) content was found to be significant in schorl (Aurisicchio et al. 1999). So far, no SIMS investigations were done in light-element analysis of axinites, but our results seem to support a role of (Fe+Mn) content, especially if Fe is present at high concentration (as in axinite 22) or is Fe^{3+} and Mn content is very high (as in axinite 47).

$Fe^{3+}/\Sigma Fe$ ratios

The contents of Fe^{3+} range from 0.00 to 0.31 apfu (samples 54 and 47, respectively), showing a semi-regular increase from ferroaxinite to manganaxinite (Table 3). Iron contents were measured as FeO_{tot} by EMPA and $Fe^{3+}/\Sigma Fe$ ratios were obtained from MS. When not enough material was available for Mössbauer spectroscopy (samples 1, 3, 14, 22, 28, and 59), the $Fe^{3+}/\Sigma Fe$ ratio was calculated from charge balance, assuming a cation total of 20.00 apfu (Table 3). This procedure was possible because, with B and H analyzed by SIMS, the Fe^{3+}/Fe^{2+} ratio was the only unmeasured variable and, as indicated by SREF, there is no evidence of cation vacancies. For samples analyzed by MS, calculated Fe^{3+}/Fe^{2+} ratios satisfactorily match experimental data (R^2 = 0.85); on average, the calculated Fe^{3+} contents (in apfu) corresponded to the measured ones within ±20% (relative). It must be noted that, if OH content is always assumed at its stoichiometric value of 2 apfu, calculated Fe^{3+} contents will be likely underestimated.

Iron-rich samples are characterized by $Fe^{3+}/\Sigma Fe$ ratios ranging from 0.00 to 0.21 (samples 54 and 35, respectively), i.e., $Fe^{2+} > Fe^{3+}$. Manganese-rich samples, in which the total Fe is very low, display a wide range of $Fe^{3+}/\Sigma Fe$ ratios (from 0.12 to 0.80, samples 58 and 47, respectively), with $Fe^{3+} > Fe^{2+}$ in nearly pure manganaxinite. An empirical relation is inferred considering total Fe content and oxidation state: the less Fe present the more it is oxidized, in agreement with the observations of Pringle and Kawachi (1980). The $Fe^{3+}/\Sigma Fe$ ratios of the present samples are definitely higher than those by MS reported in the literature, which never exceed 0.26 (Takashima and Ohashi 1968; Astakhov et al. 1975; Sonnet 1981; Pieczka and Kraczka 1994).

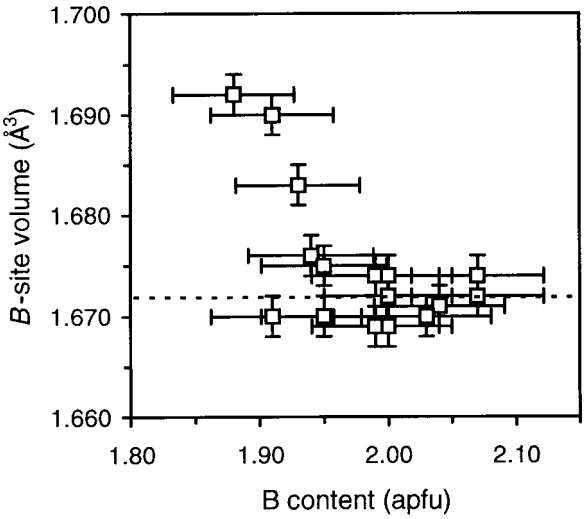

FIGURE 6. *B*-site volumes vs. B contents for axinites. Error bars: ±1σ for both *B*-site volume and B content. Dashed line: mean *B*-site volume for samples with B ≥ 1.95 apfu.

DISCUSSION

The B and OH contents derived by SIMS were compared with structural information to better evaluate the limits of their accuracy. In particular, independent confirmation of the Si → B substitution was obtained from SREF results. In the axinite structure, B occupies the *B* site, whereas Si occupies *Si*(1–4) sites (Takéuchi et al. 1974). For Si → B substitution, B < 2 apfu means that the *B* site may be partly occupied by Si. Due to the difference in cation radii between the two species (Shannon 1976), the volume of the *B* site must increase as the B content decreases. Structural data confirm this hypothesis, showing a nearly constant volume of the *B* tetrahedron for B ≥ 2 apfu, and an increase in volume for B < 2 apfu (Fig. 6). As expected, crystals with minimum B contents (e.g., samples 26, 28, 33, and 35, Table 3), have maximum values of *B*-site volume. The increase in *B*-site volumes becomes significant (>2σ) for samples with B ≤ 1.95 apfu, which corresponds to a B content 2.5% lower than the stoichiometric amount of 2 apfu. Therefore, the agreement of SIMS data with structural information may be estimated within 2.5% (relative) of the measured B content. A similar agreement of 3% between SIMS and SREF data was also observed by Hawthorne et al. (1995) measuring B in kornerupine. In both cases, of the three methods carried out on the *same* crystal fragment (EMPA, SIMS, SREF), at least two (SREF and SIMS) are completely independent, so that there can be no systematic errors common to them.

In the literature, the B content of axinite is generally assumed to be fixed but, in the few cases in which it has been measured (by classical analytical methods), B ranges from 1.7 to 2.3 apfu (Grew 1996). Although not very close to the stoichiometric value of 2 apfu (even in view of large uncertainty for B determination), these variable B contents are rather puzzling, as they do not seem to be compensated adequately by other cation substitutions.

In samples from the present study, those with a minimum B content, OH deficiency is observed to some extent, so that the charge balance for Si → B substitution is provided by the $O^{2-} \rightarrow OH^-$ substitution:

$$Si^{4+} + O^{2-} \leftrightarrow B^{3+} + OH^-, \quad \text{or} \quad SiO(BOH)_{-1}$$

The substitution of Al or Fe^{3+} for B proposed by Pieczka and Kraczka (1994) was not observed in our samples. Similarly, it was not possible to confirm the substitutions of Al for Si (Chaudhry and Howie 1969; Lumpkin and Ribbe 1979) or of Fe^{3+} for Si (Pieczka and Kraczka 1994), as the Si contents were never significantly less than stoichiometric and the MS parameters do not support the assignment of Fe^{3+} to tetrahedral coordination (Andreozzi et al., in preparation). In any case, the sum of B and Si contents is sufficient to fill all tetrahedral sites (Table 3).

The few measured OH contents of axinite reported in the literature range from 0.8 to 2.5 apfu (Deer et al. 1986). Some of these data seem of questionable accuracy, because they are commonly not consistent with bulk chemistry and charge-balance requirements. In complex minerals, OH deviations from stoichiometry are usually associated with heterovalent cation substitutions such as M^{3+} for M^{2+}. For example, one of the most common coupled mechanisms compensating for charge unbalance in tourmalines (Barton 1969; Foit and Rosenberg 1977; Gorskaya et al. 1982; Grice et al. 1993), is the following:

$$Al^{3+} + O^{2-} \leftrightarrow Fe^{2+} + OH^-, \text{ or } AlO(Fe^{2+}OH)_{-1}.$$

In a ferroaxinite, an excess of Al (> 0.5 apfu) substituting for divalent cations such as Fe^{2+} and Mg, and was charge-com-

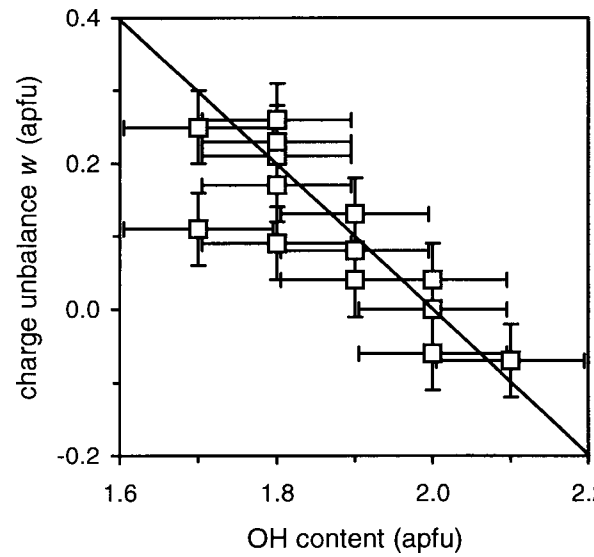

FIGURE 7. OH content vs. charge unbalance [$w = (Si - 8) + (Fe^{3+} + Al - 4)$] (apfu). Solid line with slope of –1 shows the ideal substitution. The outlier is the sample 30, with high B content.

pensated by the same amount of O^{2-} substituting for OH^- (Cassedanne et al. 1977).

In the present study, this mechanism may justify the small Al excess of sample 59 and, if slightly modified, it could also explain the Fe^{3+} excess remaining after having compensated for an eventual deficiency of Al, with this latter substitution represented by the $Fe^{3+}Al_{-1}$ vector. We found excess Fe^{3+} (substituting for divalent cations) balanced by OH deficiency in samples 1, 3, 14, 30, 38, 47, 58, and 59, corresponding to the coupled mechanism:

$$Fe^{3+} + O^{2-} \leftrightarrow Fe^{2+} + OH^-, \text{ or } Fe^{3+}O(Fe^{2+}OH)_{-1}.$$

The substitution $SiO(BOH)_{-1}$ has already been proposed for samples 26, 28, 33, and 35. For these and the previously mentioned samples, total charge unbalance w is up to 0.3 apfu and is all compensated for, within experimental error, by a comparable OH deficiency (Fig. 7).

In conclusion, on the basis of literature data and the cation substitutions observed in the study, a revised *chemical* formula for the axinite-group minerals is proposed:

$^{[6]}[Ca(Ca_{1-x}Mn_x)(Mn,Fe^{2+},Mg,Zn,Al_u,Fe^{3+}_v)_{\Sigma=1}(Al_{2-y}Fe^{3+}_y)]_2{}^{[4]}[(B_{1-z}Si_z)_2Si_8]O_{30}(OH_{1-w}O_w)_2$, where $x \le 1$, $u < 1$, $v < 1$, $y < 1$, $z << 1$, and $w = (u + v + z)$.

ACKNOWLEDGMENTS

The authors are grateful to A. Della Giusta (University of Padova) for useful comments. F.C. Hawthorne (University of Manitoba, Winnipeg) did EMP analysis of axinites A, B, and E used as references for SIMS calibration work. M. Serracino assisted during EMP analysis of axinite samples. The Museum of Mineralogy, University of Rome "La Sapienza", and its Director are thanked for allowing study of most of the samples examined here. The Natural History Museum, Smithsonian Institution, the University of Otago, R. Allori, J. Saul, L. Caserini, and L.C. de Jayasekera kindly provided the remaining samples. Ms. G. Walton revised the English text. Financial support of this work was provided by a MURST grant. Final reviews of Edward S. Grew and Frank C. Hawthorne and editorial handling of Jeffrey E. Post greatly improved the clarity and the conciseness of the paper.

REFERENCES CITED

Andreozzi, G.B. (1997) Crystal chemistry of axinites. 208 p. Ph.D. dissertation, University of Rome "La Sapienza," Rome (in Italian).

Astakhov, A.V., Voitkovskii, Yu.B., Generalov, O.N., and Sidorov, S.N. (1975) NGR investigation of some lamellar and boron-containing silicates. Soviet Physics-Crystallography, 20, 471–474.

Aurisicchio, C., Ottolini, L., and Pezzotta, F. (1999) Electron- and ion-microprobe analyses and genetic inferences on tourmalines of the foitite-schorl solid solution Elba Island (Italy). European Journal of Mineralogy, 11, 217–225.

Barton, R. Jr. (1969) Refinement of the crystal structure of buergerite and the absolute orientation of tourmalines. Acta Crystallographica, B25, 1524–1533.

Basso, R., Della Giusta, A., and Vlaic, G. (1973) Crystal structure of tinzenite. Periodico di Mineralogia, 42, 369–379 (in Italian).

Burt, D.M. (1989) Vector representation of tourmaline compositions. American Mineralogist, 74, 826–839.

Cassedanne, J.P., Cassedanne, J.O., and Estrada, N. (1977) Le gîte d'axinite de Santa Rosa (municipe de Condéuba, Etat de Bahia, Brésil). Bulletin Société Française de Minéralogie et Cristallographie, 100, 191–197.

Černý, P., Stanek, J., Novák, M., Baadsgaard, H., Rieder, M., Ottolini, L., Kavalová, M., and Chapman, R. (1995) Geochemical and structural evolution of micas in the Rozná and Dobrá Voda pegmatites, Czech Republic. Mineralogy and Petrology, 55, 177–201.

Chaudhry, M.N. and Howie, R.A. (1969) Axinites from the contact skarns of the Meldon aplite, Devonshire, England. Mineralogical Magazine, 37, 45–48.

Deer, W.A., Howie, R.A., and Zussmann, J. (1986) Axinite. In Rock-forming minerals. Disilicates and ring silicates, II ed., 629 p., Longmans, Green and Co., London.

Federico, M., Andreozzi, G.B., Lucchesi, S., Graziani, G., and Cesar-Mendes, J. (1998) Compositional variation of tourmaline in the granitic pegmatite dykes of the Cruzeiro mine, Minas Gerais, Brazil. Canadian Mineralogist, 36, 415–431.

Foit, F.F. Jr. and Rosenberg, P.E. (1977) Coupled substitutions in the tourmaline group. Contributions to Mineralogy and Petrology, 62, 109–127.

Gorskaya, M.G., Frank-Kamenetskaya, O.V, Rozhdestvenskaya, I.V., and Frank-Kamenetskii, V.A. (1982) Refinement of the crystal structure of Al-rich elbaite, and some aspects of the crystal chemistry of tourmalines. Kristallografiya, 27, 107–112.

Grew, E.S. (1996) Borosilicates (exclusive of tourmaline) and boron in rock-forming minerals in metamorphic environments. In Mineralogical Society of America Reviews in Mineralogy, 33, 387–502.

Grice, J.D., Ercit, T.S., and Hawthorne, F.C. (1993) Povondraite, a redefinition of the tourmaline ferridravite. American Mineralogist, 78, 433–436.

Hawthorne, F.C. (1996) Structural mechanisms for light-element variations in tourmaline. Canadian Mineralogist, 34, 123–132.

Hawthorne, F.C., Cooper, M., Bottazzi, P., Ottolini, L., Ercit, T.S., and Grew, E.S. (1995) Micro-analysis of minerals for boron by SREF, SIMS and EMPA: a comparative study. Canadian Mineralogist, 33, 389–397.

Ito, T., Takéuchi, Y., Ozawa, T., Araki, T., Zoltai, T., and Finney, S.S. (1969) The crystal structure of axinite revised. Proceedings of Japan Academy, 45, 490–494.

Lumpkin, G.R. and Ribbe, P.H. (1979) Chemistry and physical properties of axinites. American Mineralogist, 64, 635–645.

Ottolini, L. and Hawthorne, F.C. (1999) An investigation of SIMS matrix effects on H, Li and B ionization in tourmaline. European Journal of Mineralogy, 11(4), 679–690.

Ottolini, L., Bottazzi, P., and Vannucci, R. (1993) Quantification of lithium, beryllium, and boron in silicates by secondary ion mass spectrometry using conventional energy filtering. Analytical Chemistry, 65, 15, 1960–1968.

Ottolini, L., Bottazzi, P., Zanetti, A., and Vannucci R. (1995) Determination of hydrogen in silicates by secondary ion mass spectrometry. Analyst, 120, 1309–1313.

Pieczka, A. and Kraczka, J. (1994) Crystal chemistry of Fe^{2+}-axinite from Strzegom. Mineralogica Polonica, 25(1), 43–49.

Pringle, I.J. and Kawachi, Y. (1980) Axinite mineral group in low-grade regionally metamorphosed rocks in southern New Zealand. American Mineralogist, 65, 1119–1129.

Sanero, E. and Gottardi, G. (1968) Nomenclature and crystal chemistry of axinites. American Mineralogist, 53, 1407–1411.

Shannon, R.D. (1976) Revised effective ionic radii and systematic studies of interatomic distances in halides and chalcogenides. Acta Crystallographica, A32, 751–767.

Takashima, Y. and Ohashi, S. (1968) The Mössbauer spectra of various natural minerals. Bulletin Chemical Society of Japan, 88–93.

Takéuchi, Y., Ozawa, Y., Ito, T., Araki, T., Zoltai, T., and Finney, J.J. (1974) The $B_2Si_8O_{30}$ groups of tetrahedra in axinite and comments on deformation of Si tetrahedra in silicates. Zeitschrift für Kristallographie, 140, 289–312.

MANUSCRIPT RECEIVED JUNE 21, 1999
MANUSCRIPT ACCEPTED JANUARY 4, 2000
PAPER HANDLED BY JEFFREY E. POST